JOURNAL OF MAPS, 2018
VOL. 14, NO. 2, 45–55
https://doi.org/10.1080/17445647.2017.1422447

Taylor & Francis
Taylor & Francis Group

Science

The glacial geomorphology of upper Godthåbsfjord (Nuup Kangerlua) in southwest Greenland

Danni M. Pearce[a], Douglas W. F. Mair[b], Brice R. Rea[a], James M. Lea[b], J. Edward Schofield[a], Nicholas Kamenos[c] and Kathryn Schoenrock[d]

[a]Department of Geography, University of Aberdeen, Aberdeen, UK; [b]School of Environmental Sciences, University of Liverpool, Liverpool, UK; [c]School of Geographical and Earth Sciences, University of Glasgow, Glasgow, UK; [d]School of Natural Sciences, National University of Ireland, Galway, UK

ABSTRACT

The Greenland Ice Sheet (GrIS) is known to have experienced widespread retreat over the last century. Information on outlet glacier dynamics, prior to this, are limited due to both a lack of observations and a paucity of mapped or mappable deglacial evidence which restricts our understanding of centennial to millennial timescale dynamics of the GrIS. Here we present glacial geomorphological mapping, for upper Godthåbsfjord, covering 5800 km^2 at a scale of 1:92,000, using a combination of ASTER GDEM V2, a medium-resolution DEM (error <10 m horizontal and <6 m vertical accuracy), panchromatic orthophotographs and ground truthing. This work provides a detailed geomorphological assessment for the area, compiled as a single map, comprising of moraines, meltwater channels, streamlined bedrock, sediment lineations, ice-dammed lakes, trimlines, terraces, gullied sediment and marine limits. Whilst some of the landforms have been previously identified, the new information presented here improves our understanding of ice margin behaviour and can be used for future numerical modelling and landform dating programmes. Data also form the basis for palaeoglaciological reconstructions and contribute towards understanding of the centennial to millennial timescale record of this sector of the GrIS.

ARTICLE HISTORY
Received 10 July 2017
Revised 22 December 2017
Accepted 26 December 2017

KEYWORDS
Geomorphology; tidewater glacier; Godthåbsfjord; Greenland Ice Sheet; Little Ice Age; moraine

1. Introduction

In the early 2000s, the Greenland Ice Sheet (GrIS) experienced the largest ice-mass loss recorded in the instrumental record, largely attributed to increased surface melting (Hanna et al., 2013) and enhanced ice discharge from accelerating marine/fjord terminating outlets (Amundson et al., 2010; Howat, Box, Ahn, Herrington, & McFadden, 2010). Compared to the east coast of Greenland, the west has exhibited strong warming associated with changes in summer general circulation (Van As et al., 2014). Despite this warming trend, the land-terminating glacier outlets are currently experiencing a regional slowdown in recession (Tedstone et al., 2015), whereas tidewater glaciers have generally increased in velocity and undergone significant retreat (Joughin et al., 2008; Kjeldsen et al., 2015; Motyka et al., 2017; Murray et al., 2010; Van den Broeke et al., 2009).

Satellite imagery recorded since the 1970s has facilitated the reconstruction of glacier fluctuations in west Greenland, but prior to this, estimating the spatial and temporal changes is rather more challenging due to the sparse proxy records and lack of direct observations (Lea, Mair, Nick, Rea, van As, et al., 2014; Lea, Mair, Nick, Rea, Weidick, et al., 2014). The record has been extended to the century timescale by employing historical maps, written accounts, aerial photos from the 1930s onwards and the identification of Little Ice Age (LIA;*c.* AD 1300–1850) extent from remotely sensed imagery (e.g. Kjeldsen et al., 2015). Reconstructions over these timescales are extremely important when contextualising the present dynamic changes, because the length of the observational record makes it difficult to capture glacial behaviour that acts on centennial to millennial scales. Thus, current high-resolution observational data may be biased towards short-term fluctuations (Vieli & Nick, 2011), rather than longer term response to climate forcing. This, in addition to their nonlinear response to climate forcing could lead to inaccurate mass loss projections and concomitant contributions to future sea-level rise (Nick, Vieli, Howat, & Joughin, 2009). Predicting the responses of both land and tidewater glaciers is crucial given the current unprecedented warming trend (Andresen et al., 2012; Khan et al., 2015). We present a glacial geomorphological map, associated with land-terminating and tidewater glaciers, located in upper Godthåbsfjord, SW Greenland, which can be used to contexulise the present-day changes.

CONTACT Danni M. Pearce d.pearce@abdn.ac.uk
Supplemental data for this article can be accessed at https://doi.org/10.1080/17445647.2017.1422447

2. Study area

Godthåbsfjord (Nuup Kangerlua) in southwest Greenland (*c.* 64–65°N, 49–51°W) is one of the largest fjord systems in the world. It is *c.* 190 km in length, up to 7 km wide and covers a total area of *c.* 2013 km^2 (Figure 1). The uppermost branch of Godthåbsfjord, Kangersuneq, is located approximately 80 km inland from the coast and connects the marine environment to the margin of the GrIS. Six outlets drain this sector of the ice sheet and reach sea level, or close to sea level. Of these, three ice sheet outlets terminate on land, with extensive sandur plains in front of their termini. These are (from north to south): Kangilinnguata Sermia (KS), Qamanaarsuup Sermia (QS) and Kangaasarsuup Sermia (KSS). A further three ice sheet outlets terminate in marine conditions: Narsap Sermia (NS), Akullersuup Sermia (AS) and Kangiata Nunaata Sermia (KNS). Surrounding bedrock covers ~80% of the mapped area, and is predominantly composed of Archaean Gneiss (*c.* 3900–3600 Ma yr) with the tectonic fabric approximately SW to NE (Henriksen, Higgins, Kalsbeek, & Pulvertaft, 2000). The fjord landscape has an arborescent configuration with numerous branches and outlets. Mountain summits are typically between 500 and 1480 m above sea level (a.s.l.), with steep valley sides mostly in excess of *c.* 30°. Typically,

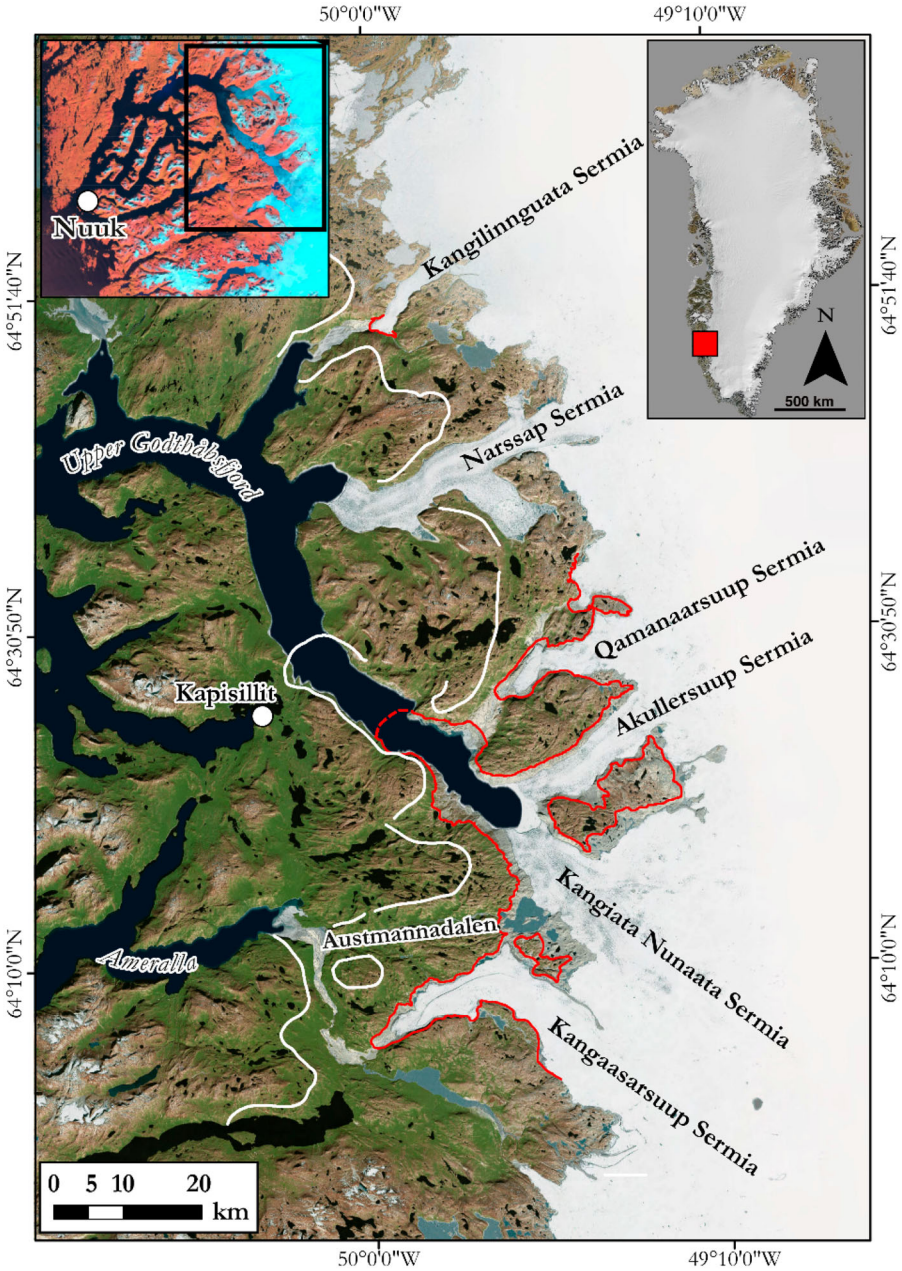

Figure 1. (Main panel) Aerial map of upper Godthåbsfjord showing outlets from the GrIS. The red line indicates the approximate extent of the outlets during the LIA (redrawn from Weidick, Bennike, Citterio, & Nørgaard-Pedersen, 2012). The white line indicates the locations of the Kapisillit moraines (redrawn from Weidick et al., 2012 and Larsen et al., 2014). (Inset, top left) Landsat image (2013) of the wider fjord system into which Godthåbsfjord is connected with. The capital of Greenland, Nuuk, is labelled. The black box denotes the mapped area featured in this study. (Inset, top right) Location of the study area in Greenland.

interconnected lakes are present in the valley floors, whilst numerous smaller bedrock controlled lakes can be found at higher altitudes.

3. Brief glacial history

During the Last Glacial Maximum the ice sheet in West Greenland extended onto the continental shelf and began to disintegrate ~17 cal ka BP (Knutz, Sicre, Ebbesen, Christiansen, & Kuijpers, 2011). Around coastal areas, the early Holocene glacial history is relatively well known. Larsen et al. (2014) proposed a rapid and early deglaciation from the coast, between 11.4 and 10.4 cal ka BP. Inland of this and within the study area, approximately 10–30 km from the present-day ice margin, prominent moraines (also referred to as the Kapisillit [old orthography: Kapisigdlit] moraines, Figure 1), are thought to mark a major standstill, or readvance of the ice sheet somewhere between 10.4 and 8.2 ka cal BP (Beschel, 1961; Larsen et al., 2014; Weidick et al., 2012). It is currently uncertain if the moraines formed during one or several events but it is feasible that these features correlate to the Fjord Stade moraines found to the north, around Disko Bugt, and they may be indicative of widespread early Holocene moraine formation (Young et al., 2013) More is known about late Holocene outlet fluctuations largely because in upper Godthåbsfjord the outlets, in particular tidewater glaciers, have all experienced retreat since the LIA maximum around the mid-eighteenth century (Taurisano, Billionøggild, & Karlsen, 2004; Taurisano, Bøggild, Schjøth, & Jepsen, 2003). To assess these changes emphasis has typically been placed upon historical information, initiated by Weidick (1959, 1963) and Weidick et al. (2012), who reviewed glacier change using secondary sources and disparate descriptions of ice-marginal features. Recent studies have tended to focus on KNS, with mapping of trimlines and moraines demonstrating the outlet has undergone a staged retreat of >22 km since its LIA maximum in 1721 (Lea, Mair, Nick, Rea, van As, et al., 2014; Lea, Mair, Nick, Rea, Weidick, et al., 2014) with a standstill, or readvance, occurring between 1859 and 1920 (Lea, Mair, Nick, Rea, van As, et al., 2014; Weidick et al., 2012) (Figure 1). Consequently, KNS is the largest and most dynamic tidewater glacier south of Jakobshaven Isbræ and, despite the non-linear response to climate, has been sensitive to changes in climate since the LIA (Lea, Mair, Nick, Rea, van As, et al., 2014; Lea, Mair, Nick, Rea, Weidick, et al., 2014).

4. Methods

Glacial landforms were identified and mapped using two forms of remote sensing data and panchromatic aerial orthophotographs, alongside ground truthing which took place during a total of six weeks of fieldwork in 2015 and 2016. Google Earth was used for 3D landform visualisation and reconnaissance of valleys/landforms prior to field work.

Advanced Spaceborne Thermal Emission and Reflection Radiometer (ASTER) global (GDEM V2) data (https://asterweb.jpl.nasa.gov/gdem.asp), gridded to 30 m^2 resolution, was used as a first pass. At this resolution only the largest glacial features, such as troughs, were visible on the DEM (Figure 2(A)) and so a medium-resolution DEM was used to complement the GDEM (Korsgaard, Nuth, Khan, Kjeldsen, Anders, et al., 2016; Korsgaard, Nuth, Khan, Kjeldsen, Bjørk, et al., 2016) (Figure 2(B)). Based on a 1985 aerial survey conducted by the Agency for Data Supply and Efficiency (previously the Danish Geodata Agency), this DEM had an associated ground control (GR96) and error <10 m horizontal and <6 m vertical accuracy (https://data.nodc.noaa.gov/cgi-bin/iso?id=gov.noaa.nodc:0145405). The medium resolution DEM data set was converted into a hillshade relief model, illuminating from 315° to 45° to avoid azimuth biasing, using the Spatial Analyst function in ESRI ArcGIS 10, for meaningful graphical and analytical purposes (Ely, Gribble, & Clark, 2016; Paine & Kiser, 2012; Pearce, Rea, Bradwell, & McDougall, 2014). This enabled a rapid assessment of the terrain, and evaluation of large-scale glacial landforms, such as streamlined bedrock and well-developed meltwater channels (several kilometres in length and *c.* 0.5 km in width) and prominent moraines (Figure 2(C,D)). The ASTER GDEM was not used under a hillshade rendition because terrain became too coarse at this scale to view landforms. For this region, particular care was taken when identifying glacial meltwater channels as it is likely that the channels will have exploited bedrock faults. Meltwater channels were therefore identified as glacial in origin where there was discordance with modern day fluvial drainage patterns and they were mapped along their thalweg (cf. Domack, Amblas, & Canals, 2016; Ely, Gribble, et al., 2016; Greenwood, Clark, & Hughes, 2007).

Smaller-scale features measuring tens of metres which were not visible on the DEMs, were mapped using one set of digital panchromatic orthophotographs (hereafter referred to as aerial photographs) from 1985, with a nominal ground resolution of between 2.1 and 2.25 m (Korsgaard, Nuth, Khan, Kjeldsen, Bjørk, et al., 2016; data from https://data.nodc.noaa.gov/cgi-bin/iso?id=gov.noaa.nodc:0145405) (Figure 2(E)). This digital dataset, supplied in ESRI shapefiles and projection format, enabled identification of landforms, in particular, moraines, trimlines, lake shorelines and sediment lineations. Moraines were mapped as polylines along their crest and were easily identified as positive features. Trimlines were mapped along the difference in terrain; for example,

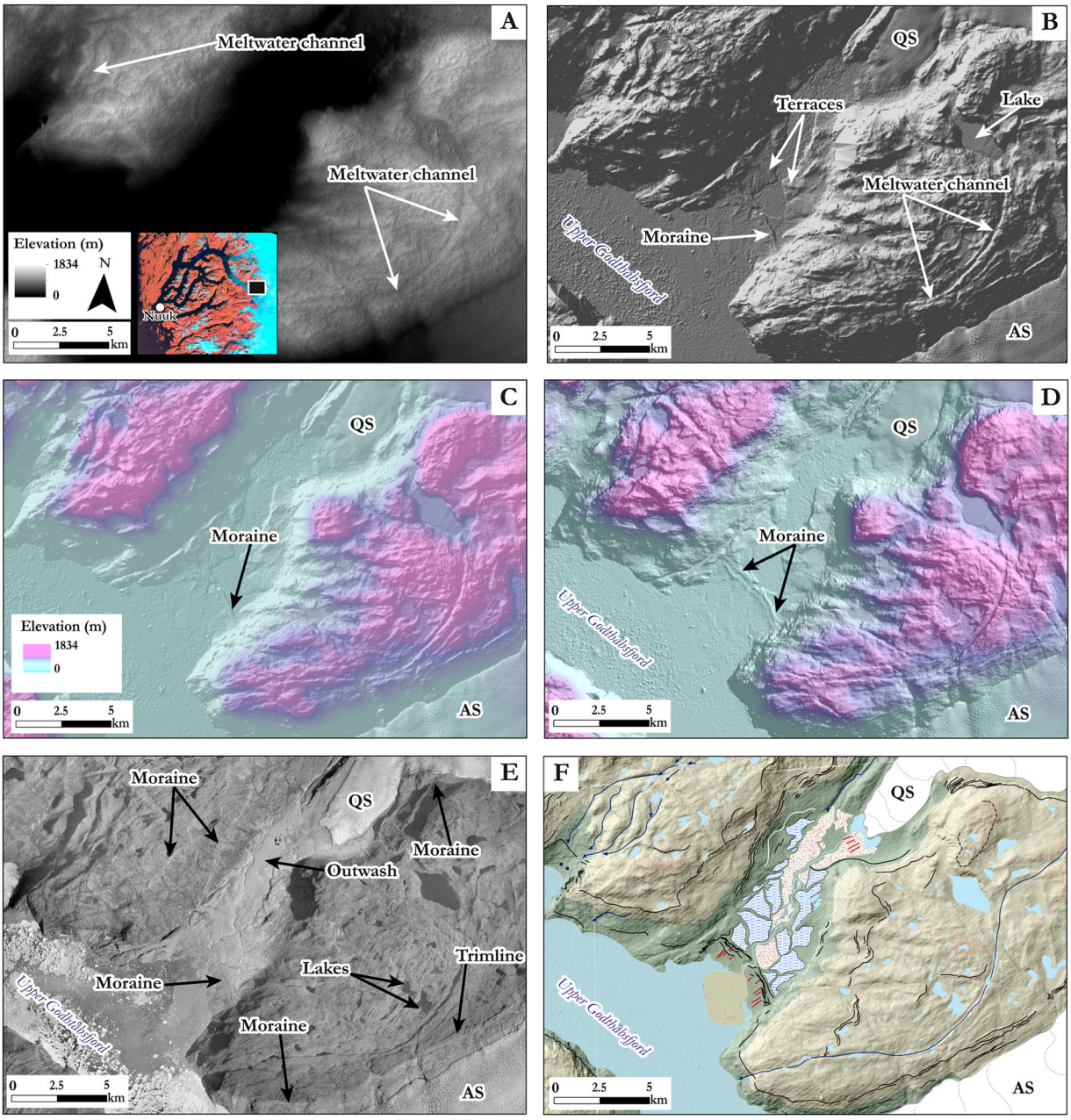

Figure 2. Example of the mapping process for Qamanaarsuup Sermia (QS). (A) As a first pass, negative features, such as meltwater channels, were mapped from the ASTER GDEM V2. (B) Hillshade relief model produced using the medium resolution DEM (Korsgaard, Nuth, Khan, Kjeldsen, Anders, et al., 2016; Korsgaard, Nuth, Khan, Kjeldsen, Bjørk, et al., 2016). Under this rendition, more landforms were visible including the outlets QS and AS, moraines, lakes and terraces. (C) Hillshade relief model, derived from B, using an azimuth of 315° and (D) 45° with both having an illumination of 30°. It can been seen from D the change in azimuth highlights the moraine in more detail. (E) Panchromatic orthophotographs from Korsgaard, Nuth, Khan, Kjeldsen, Anders, et al. (2016) and Korsgaard, Nuth, Khan, Kjeldsen, Bjørk, et al. (2016), which enabled higher resolution mapping of moraines, trimlines and smaller lakes that could not be identified solely from the DEMs. (F) Final map production using datasets A to E with mapping overlain on the hillshade DEM. The polygon fills are presented in a different colour to the Main Map for clarity when viewed at this scale.

where there was a clear change from ice-moulded topography to vegetation, a polyline was mapped along this sharp change. Similarly, lake shorelines were identified based upon their sharp break of slope, which followed the same geometry as the contemporary lake level and appeared as sequences resulting from gradual lake level lowering. The reliability mask produced by Korsgaard, Nuth, Khan, Kjeldsen, Bjørk, et al. (2016) was used to check shadowed areas on the aerial photographs and these coincided with either steep cliff sections or lakes and therefore did not affect the mapping.

A repeat pass approach to landform mapping was taken where an iterative process, conducted by a single user involving numerous consultations between the datasets, was undertaken before final interpretations were decided upon (Ely, Gribble, et al., 2016; Pearce et al., 2014; Smith & Wise, 2007) (Figure 2(F)). This proved particularly useful when mapping sediment lineations and streamlined bedrock, since the former

were only visible on the aerial photographs and are often draped over the streamlined bedrock, which was only visible when using the DEMs alongside the aerial photographs (Bradwell, 2005; Lane, Roberts, Rea, Ó Cofaigh, & Vieli, 2015).

5. Map production

The production of the Main Map utilised all the techniques discussed above and was produced using ESRI ArcGIS 10.2. In general, it was also noted that landform preservation decreases with distance from the contemporary ice sheet margin. For example, numerous ice-marginal positions adjacent to AS were easily identified compared to the terrain to the far west of Austmannadalen. As a result, a limitation of the final map production is that some areas were mapped in considerably more detail than others. Although landform preservation influences the spatial density of the mapped landforms, it should be noted that smaller features, which are below the resolution of the remote data, could be identified through further field mapping.

On the Main Map, the mapped moraines and other landforms are draped over the medium-resolution DEM (Korsgaard et al., 2016) set with a 25% transparency. To provide a more aesthetic background for the geomorphology this DEM is underlain with a classified DEM and colour ramp (Figure 2(F)). Adding terrain shading is not only visually pleasing, but also provides the end user with a much better idea of local height differences and the nature of the terrain, than can be derived from a height–colour scale alone. However, although it aids the end user in understanding the map content, given that two independent spatial datasets are used with different elevation accuracies, the DEM is for illustrative purposes only.

Contemporary lakes were easily mapped due to their visibility as changes in break of slope (Spagnolo et al., 2014). Exceptions to this were ice-dammed lakes located near to the ice margins of NS and KNS, for example, Isvand, which is located to the southwest of KNS has periodically drained, subglacially, since 2004 (Weidick & Citterio, 2011). Consequently, the lake level from the 1985 aerial photographs (i.e. prior to initiation of lake level fluctuation) was mapped (Figure 3(A,B)), and a representative contemporary lake extent was derived from Landsat 7 imagery (acquired 10th July 2013). In addition, a number of ice-marginal lakes (<500 m in width) were identified at the (1985) ice sheet margin, (e.g. adjacent to NS ice margin), which have also since drained (Kjeldsen et al., 2014). As a result, only their 1985 extent is represented on the Main Map.

Both the ASTER DEM and the medium-resolution DEM depict the ice sheet margins at their extent in 1985, and so this was mapped with a polyline (Figure 3(B)). To map more recent ice sheet extent, the margins were derived using the 15 m panchromatic scenes (Band 8) from Landsat 7, which was acquired in 2013. The map is projected in WGS 1984 UTM Zone 22N and is designed to be printed on A0 paper at a scale of 1:92,000. In addition, locations with a higher number of glacial landforms can be viewed at 1:25,000. The DEM becomes increasingly pixelated at this scale, but this does not affect the vector-based polylines/polygons. The Main Map was exported in PDF format.

6. Landforms

6.1. Moraines and trimlines

Prominent ridges are interpreted as moraines based upon their positive morphology as long continuous and discontinuous tracts of sediment along the valley sides. A range of moraine sizes were observed, the smallest being <2 m high and a few metres in length (which is at the limit of the resolution of the datasets being used) and increasing to tens of metres in height and several kilometres in length. Three sets of moraines were identified based on their morphology, number of crestlines mapped and relative distance to the present ice margin. The first and outermost set (Set 1) was identified as a discontinuous ridges *c.* 15 km west of KNS and KSS, extending from *c.* 200 to 880 m a.s.l. (Figure 4(A,B)). Large well-developed moraines are also found on the terrain above QS and KS. The moraines identified as Set 1 correspond to the Kapisillit moraines defined in earlier studies (Larsen et al., 2014; Weidick et al., 2012). No further moraines were identified beyond this from the remote datasets, although, it is likely that additional smaller moraines could be identified from ground investigations.

A second set of moraines (Figure 4(A,C); Set 2) is located *c.* 9 km inside the first set. Lower in elevation (150–650 m a.s.l.), these moraines can often be linked to trimlines defining former ice-marginal positions. The preservation and near continuous nature of these moraines, and their more densely vegetated distal surfaces, are features indicative of formation during the LIA (Kjeldsen et al., 2015; Lea, Mair, Nick, Rea, Weidick, et al., 2014; Weidick et al., 2012). The most well-developed moraines and trimlines are found at KNS, KSS and AS, whilst there are only discontinuous trimlines associated with QS, NS and KS. Paraglacial modification is prominent on the lateral moraines, such as south of KNS, which display regions of intensive gullying. This creates a hummocky topography as the sediment is reworked to a lower elevation.

The third set of moraines (Figure 4(A,C)) is located *c.* 600 m lower in elevation than Set 2 and in the upper parts of the valleys these moraines connect to the present ice margin. The clearest moraines are associated

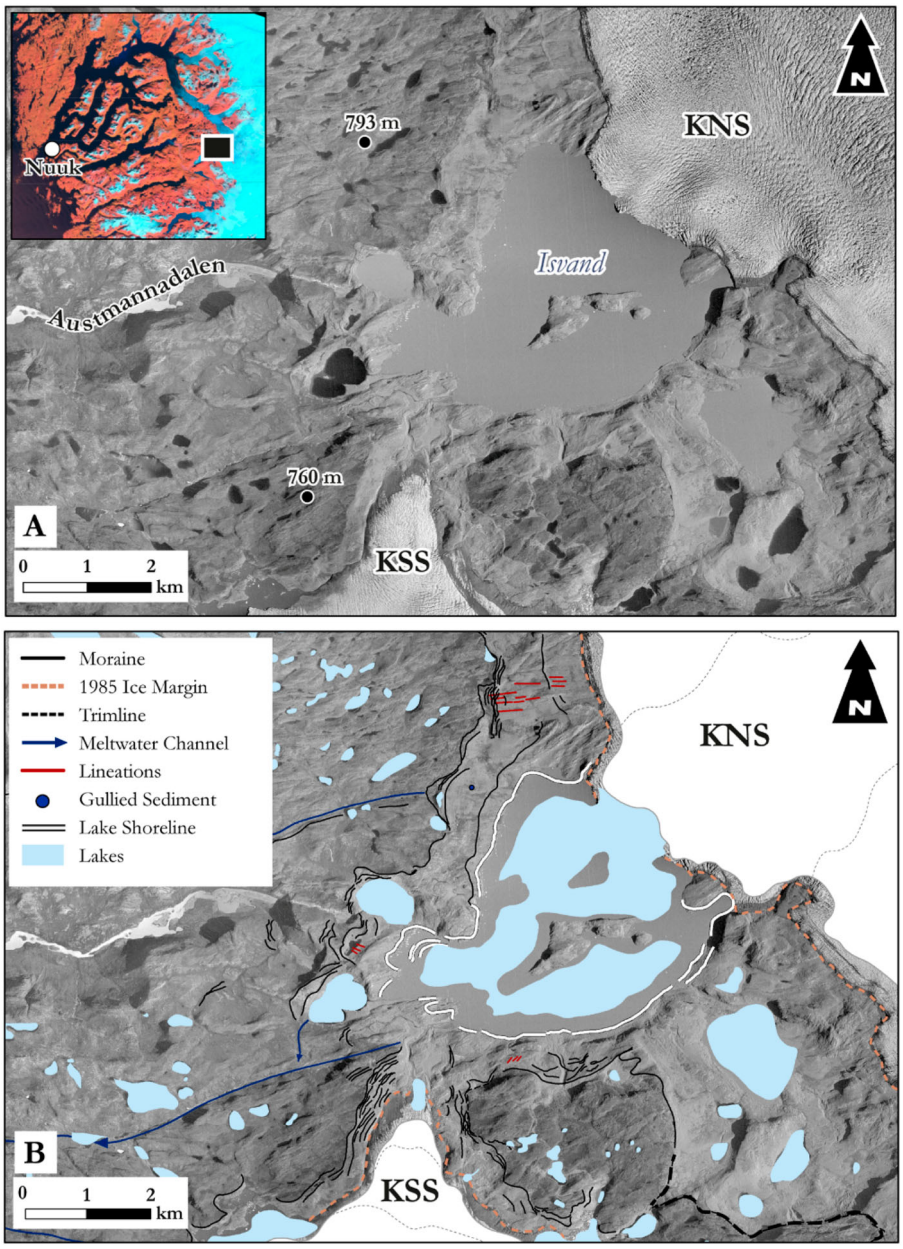

Figure 3. Mapping of the ice-dammed lake Isvand and the ice margins associated with KNS and KS. (A) Aerial photograph depicting the 1985 extent of Isvand and the ice sheet. (Inset A) Landsat image of the Godthåbsfjord system and the capital Nuuk. The box denotes the area covered by the larger panels. (B) Geomorphological mapping using A. The lake shorelines produced by Isvand in 1985 are denoted by the white lines. The 2013 (reduced) extent of the lake is shown in blue.

with southern valley side of KNS, where a continuous lateral moraine can be traced up-valley for *c.* 11 km where it terminates at the ice-dammed lake Isvand (Figure 4(A,C)). Numerous smaller moraines are spatially aligned forming down-valley chains, sometimes curving arcuately towards the former ice margin. This configuration indicates that the moraines reflect former ice-marginal positions of actively retreating outlets (Boston, 2012; Lukas & Bradwell, 2010; Pearce, 2014).

6.2. Lineations and streamlined bedrock

The term 'lineation' is used here in reference to landforms composed of sediment which have been formed in the subglacial environment and are aligned with the direction of ice flow. The lineations are positive, elongate features, which range from tens of metres to approximately 300 m in length, and are several metres in height. Examples are found around the margin of KNS (Figure 5(A,C)), in the proglacial area of QS to and to the north of Tummeralik (Figure 4(A)). Additionally, examples of glacially streamlined bedrock were mapped to the north of Tummeralik and between AS and KNS (Figure 5(A,B)). These features were morphologically different to lineations because they were identified on the panchromatic aerial photographs as being composed of bedrock, rather than sediment. The streamlined bedrock features are also larger, often being ≤10 km in length. The streamlining was distinctive since there is an abrupt transition between

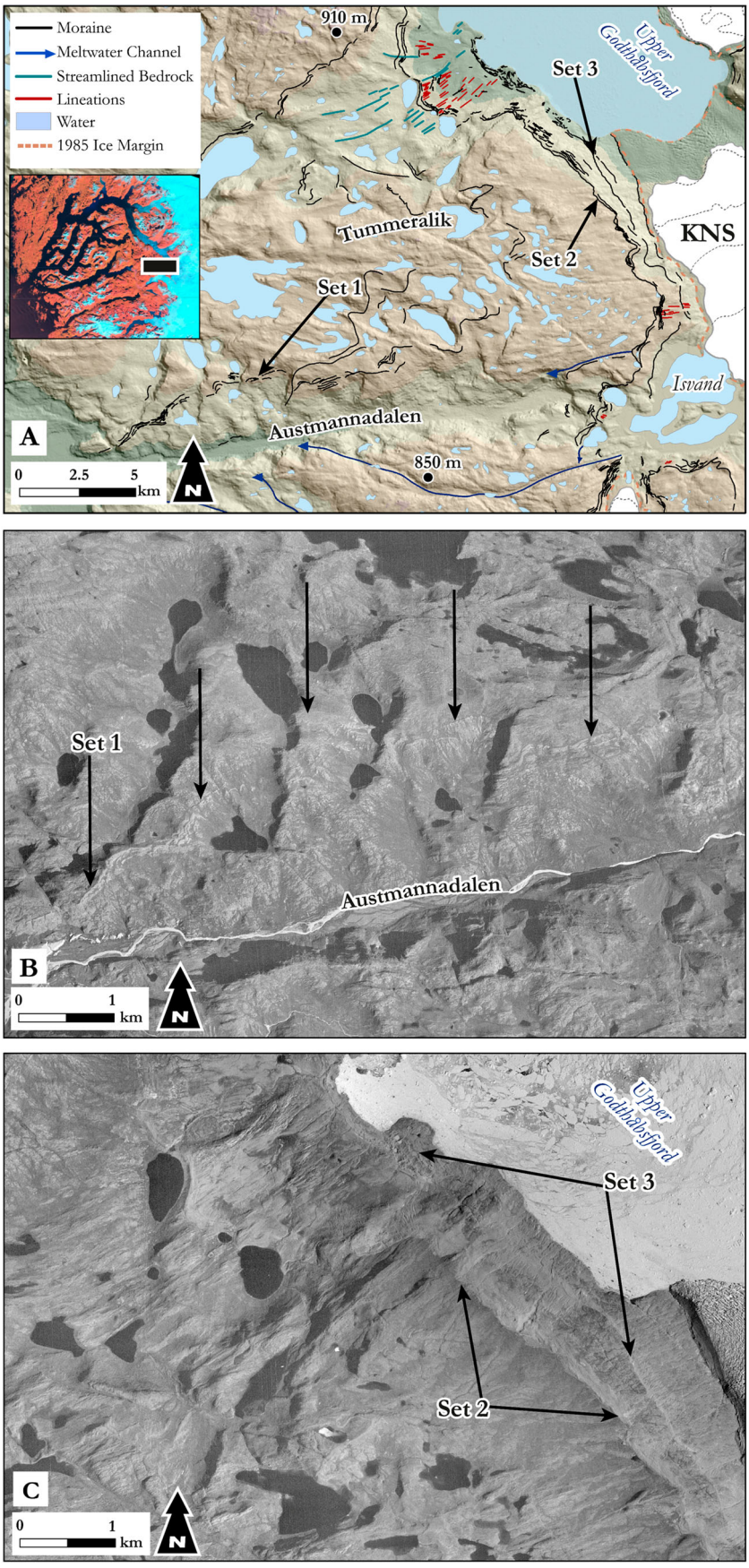

Figure 4. Example of mapped moraines. (A) The geomorphological map, overlain on the medium-resolution DTM, showing the three sets of moraines identified in Upper Godthåbsfjord (Set 1 to 3). Some map layers have been omitted to make the image legible at this scale. (Inset A) Landsat image of the Godthåbsfjord system with the box showing the location of the area covered by the larger panels. (B) Aerial photographs of the Set 1 moraines above the valley of Austmannadalen. (C) Aerial photographs of the moraines associated with Sets 2 and 3. Black arrows highlight the moraines. Their locations approximately correspond to those in A.

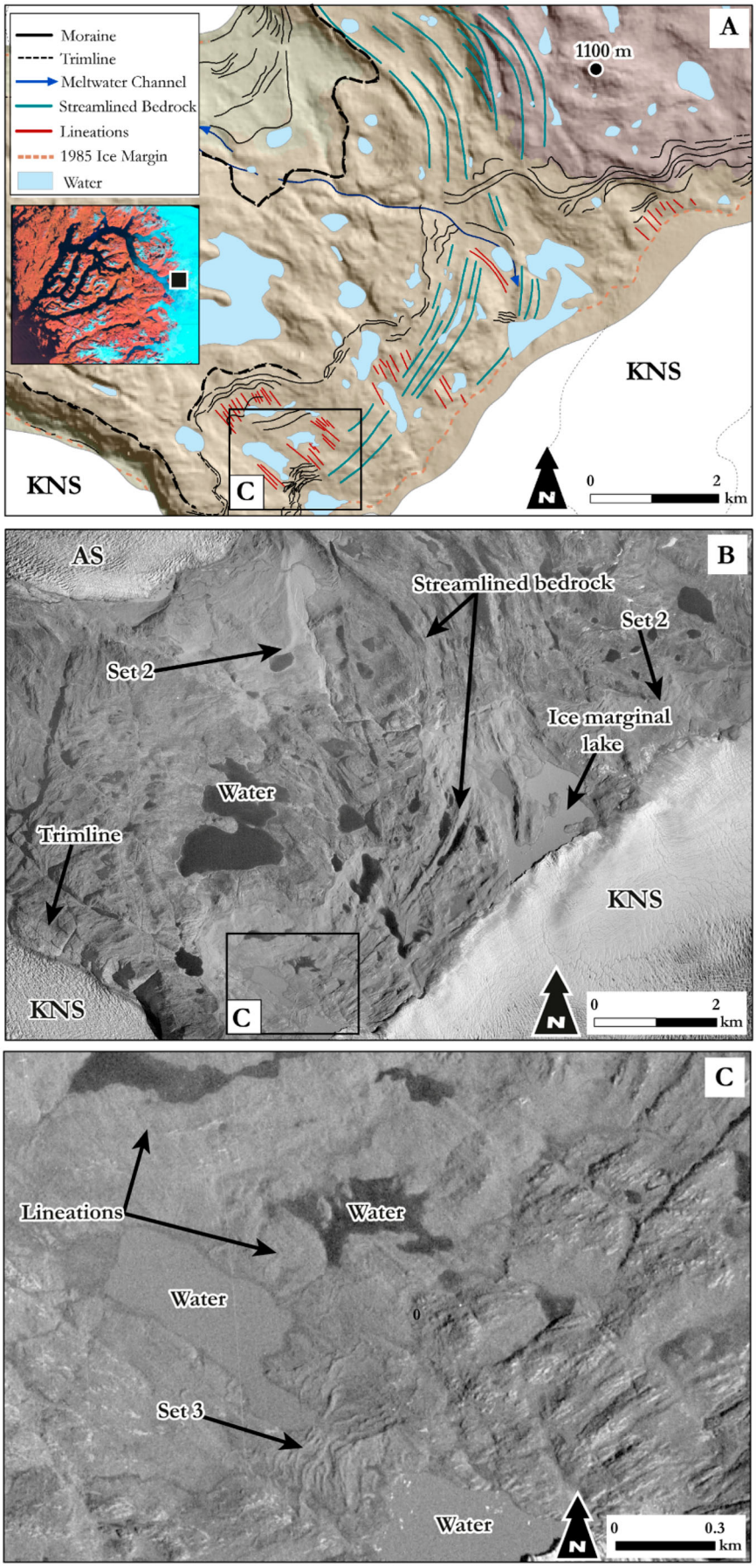

Figure 5. Example of lineations and streamlined bedrock. (A) The geomorphological map, overlain on the medium-resolution DTM. Some map layers have been omitted to make the image legible at this scale. (Inset A) Landsat image of the Godthåbsfjord system and with the box showing the location of the area covered by the larger panels. (B) Aerial photographs of the streamlined bedrock, Set 2 moraines and an ice-marginal lake, which has subsequently drained (after 1985). (C) Aerial photographs of the lineations, which are composed of sediment and Set 3 moraines.

elongate streamlined bedrock around AS and KNS, which trends approximately north–south, and the adjacent bedrock which shows no signs of modification. In this area, the streamlined bedrock has a cross-cutting relationship with the sediment lineations, which are superimposed on top of bedrock indicating the lineations were formed subsequent to bedrock streamlining (Figure 5). Both landforms may be utilised to infer past ice-flow direction (e.g. Hughes, Clark, & Jordan, 2010; Lane et al., 2015).

6.3. Fluvial and glaciomarine features

Lateral meltwater channels, marking the likely position of the former ice margin, were identified at altitudes (500–700 m) following the criteria by Greenwood et al. (2007). They possess oblique down-slope profiles parallel to the valley sides and their overall pattern formed flights of discontinuous, lateral channels, revealed on the DEMs from the successive negative features on the valley sides. Larger subglacial meltwater channels, *c.* 11 km in length and 40 m in width, were identified following descriptions by Glasser and Bennett (2004) and Nitsche, Larter, Gohl, Graham, and Khun (2016). The channels differ from lateral meltwater channels because they are sinuous features deeply incised into the bedrock and disregard structural lineaments. An example of this is found on the high ground between QS and AS (Figure 5).

Larger ice-dammed lakes are found around NS and KNS and were easily identified from the aerial photographs due to a change in reflectance and the horizontal lake surface level. In particular, Isvand to the southwest of KNS is known to have changed its meltwater routing in relation to the KNS ice margin (e.g. Weidick & Citterio, 2011), leaving a number of mappable lake shorelines. In addition, palaeo-ice dammed lakes were identified to the north of Tummeralik from the successive abandoned shorelines on the valley side at 247–322 m a.s.l. Another palaeo-ice dammed lake to the south of QS and described by Weidick et al. (2012) was mapped from discontinuous shorelines at *c.* 61 m a.s.l., below which dissected lake sediments are present. These were identified from the panchromatic aerial photographs through a clear difference between the light coloured sediment and the darker vegetated valley sides. The palaeo-ice dammed lakes formed when KNS was at its LIA maximum (Lea, Mair, Nick, Rea, Weidick, et al., 2014) and provide an opportunity to constrain the advance of KNS through absolute dating techniques (e.g. by radiocarbon dating of plant macrofossils that represent the *in situ* vegetation prior to flooding; these are now exposed in open sections within organic deposits below the lake sediments).

A number of glaciomarine features are present and can be found adjacent to the present fjords, or elevated above the valley floor. An isolated ridge, to the north of Kapisillit, represents a local marine limit at *c.* 50 m a.s.l. Approximately 9 km north of this is a series of raised shorelines, which have formed *c.* 18 km beyond the LIA moraines, and extend up to an elevation of *c.* 90 m a.s.l. To the south of this, at the entrance to Austmannadalen, there are multiple outcrops of fine-grained glaciomarine silts which contain shell casts and extend up-valley for *c.* 5 km, plus two terraces/delta tops are located at approximately 2.5 km from the valley entrance. While no glaciomarine exposures were found to examine, it seems probable that the delta top is related to the glacial high stand and represents the local marine limit at *c.* 90 m a.s.l. Placed into a wider context, Sisimiut (to the north of the study area) experienced more isostatic rebound with a higher marine limit of 140 m a.s.l., whilst south of Nuuk the marine limit is lower 50 m a.s.l. (Kelly, 1985; Woodroffe, Long, Lecavalier, Milne, & Bryant, 2014). It is feasible that other glaciomarine features are present in the area, but their subtle nature creates difficulties in delineating them when mapping using remote datasets. However, accurate recording may be achieved through field mapping and ground truthing.

7. Conclusions

Numerous glacial landforms associated with both the land terminating and tidewater glaciers in upper Godthåbsfjord have been identified and mapped. Landforms include a large number of moraines and trimlines – found both along the valley sides and extending up and onto the higher terrain – that indicate former ice-marginal positions, and lineations, streamlined bedrock, meltwater channels and glaciomarine features. The identification of palaeo-ice dammed lakes provides evidence that can be used to help constrain the timing of advance of KNS to its LIA maximum. This is the first detailed regional map of the glacial geomorphology in the upper Kangersuneq fjord system and it provides the basis for a future empirical reconstruction of the behaviour of this portion of the GrIS as crucial data for numerical model validation.

Software

ESRI ArcGIS10.2 was used to view, manipulate and undertake mapping.

Acknowledgements

We would like to thank Jasper Knight, Samuel Kelley, Niels Jákup Korsgaard and Makram Murad-al-shaikh for their constructive and insightful reviews which improved this article. We would also like to extend our thanks to the GINR for their time and field support in 2015 and 2016.

Disclosure statement

No potential conflict of interest was reported by the authors.

Funding

This research project, Calving glaciers: Longterm validation and evidence (CALVE), was funded by the Leverhulme Trust under grant number RG-12099-10. JL would like to acknowledge the British Geomorphological Society and Quaternary Research Association for supporting fieldwork undertaken in 2015. DP would like to acknowledge the NERC Geophysical Equipment Facility for their equipment loan (GEF1049) as well as time and advice offered whilst in the field.

References

Amundson, J. M., Fahnestock, M., Truffer, M., Brown, J., Lüthi, M. P., & Motyka, R. J. (2010). Ice mélange dynamics and implications for terminus stability, Jakobshaven Isbræ, Greenland. *Journal of Geophysical Research*, *115*, 33729. doi:10.1029/2009JF001405

Andresen, C. S., Straneo, F., Ribergaard, M. H., Bjørk, A. A., Andersen, T. J., Kuijpers, A. … Ahlstrøm, A. P. (2012). Rapid response of Helheim Glacier in Greenland to climate variability over the past century. *Nature Geoscience*, *5*, 37–41. doi:10.1038/ngeo1349

Beschel, R. E. (1961). Dating rock surfaces by lichen growth and its application to glaciology and physiography (lichenometry). In G. O. Raasch (Ed.), *Geology of the Arctic, proceedings of the first international symposium on Arctic geology* (Vol. 2, pp. 1044–1062). Calgary, Alberta.

Boston, C. M. (2012). A glacial geomorphological map of the Monadhliath Mountains, central Scottish Highlands. *Journal of Maps*, *8*(4), 437–444. doi:10.1080/17445647.2012.743865

Bradwell, T. (2005). Bedrock megagrooves in Assynt, NW Scotland. *Geomorphology*, *65*(1), 195–204. doi:10.1016/j.geomorph.2004.09.002

Domack, E. W., Amblas, D., & Canals, M. (2016). Bedrock meltwater channels in Palmer Deep, Antarctic Peninsula. In J. A. Dowdeswell, M. Canals, M. Jakobsson, B. J. Todd, E. K. Dowdeswell, & K. A. Hogan (Eds.), *Atlas of submarine glacial landforms: Modern, quaternary and ancient* (Vol. 46, pp. 211–212). London, Memoirs: Geological Society. doi:10.1144/M46.

Ely, J. C., Gribble, E. A., & Clark, C. D. (2016). The glacial geomorphology of the western cordilleran ice sheet and Ahklun Ice Cap, Southern Alaska. *Journal of Maps*, *12* (51), 415–424. doi:10.1080/17445647.2016.1234981

Glasser, N. F., & Bennett, M. R. (2004). Glacial erosional landforms: Origins and significance for palaeoglaciology. *Progress in Physical Geography*, *28*(1), 43–75. doi:10.1191/0309133304pp401ra

Greenwood, S. L., Clark, C. D., & Hughes, A. L. (2007). Formalising an inversion methodology for reconstructing ice-sheet retreat patterns from meltwater channels: Application to the British Ice Sheet. *Journal of Quaternary Science*, *22*(6), 637–645. doi:10.1002/jqs.1083

Hanna, E., Navarro, F. J., Pattyn, F., Domingues, C. M., Fettweis, X., Ivins, E. R., … Zwally, H. J. (2013). Ice-sheet mass balance and climate change. *Nature*, *498*, 51–59. doi:10.1038/nature12238

Henriksen, N., Higgins, A. K., Kalsbeek, F., & Pulvertaft, T. C. R. (2000). Crystalline rocks older than 1600 Ma: The Greenland Precambrian shield. In N. Henriksen, A. K. Higgins, F. Kalsbeek, & T. C. R. Pulvertaft (Eds.), *Greenland from Archaean to Quaternary. Descriptive text to the Geological map of Greenland, 1:2 500 000* (Vol. 185, pp. 12–24) (2nd ed.). Geological Survey of Denmark and Greenland Bulletin 18. Copenhagen: Geologicial Survey of Denmark and Greenland.

Howat, I. M., Box, J. E., Ahn, Y., Herrington, A., & McFadden, E. M. (2010). Seasonal variability in the dynamics of marine-terminating outlet glaciers in Greenland. *Journal of Glaciology*, *56*(198), 601–613. doi:10.3189/002214310793146232

Hughes, A. L., Clark, C. D., & Jordan, C. J. (2010). Subglacial bedforms of the last British Ice Sheet. *Journal of Maps*, *6* (1), 543–563. doi:10.4113/jom.2010.1111

Joughin, I., Howat, I. M., Fahnstock, M., Smith, B., Krabill, W., Alley, R. B., … Truffer, M. (2008). Continued evolution of Jakobshavn Isbræ following its rapid speedup. *Journal of Geophysical Research*, *113*, F04006. doi:10.1029/2008JF001023

Kelly, M. (1985). A review of the quaternary geology of Western Greenland. In J. T. Andrews (Ed.), *Quaternary environments in Eastern Canadian Arctic, Baffin Bay and Western Greenland* (pp. 461–501). Boston, MA: Allen and Unwin.

Khan, S. A., Aschwanden, A., Bjørk, A. A., Wahr, J., Kjeldsen, K. K., & Kjær, K. H. (2015). Greenland ice sheet mass balance: A review. *Reports on Progress in Physics*, *78*, 046801. doi:10.1088/0034-4885/78/4/046801

Kjeldsen, K. K., Korsgaard, N. J., Bjørk, A. A., Khan, S. A., Box, J. E., Funder, S., … Kjær, K. H. (2015). Spatial and temporal distribution of mass loss from the Greenland Ice Sheet since AD 1900. *Nature*, *528*, 396–400. doi:10.1038/nature16183

Kjeldsen, K. K., Mortensen, J., Bendtsen, J., Petersen, D., Lennert, K., & Rysgaard, S. (2014). Ice-dammed lake drainage cools and raises surface salinities in a tidewater outlet glacier fjord, west Greenland. *Journal of Geophysical Research: Earth Surface*, *119*, 1310–1321. doi:10.1002/2013JF003034

Knutz, P. C., Sicre, M. A., Ebbesen, H., Christiansen, S., & Kuijpers, S. (2011). Multiple-stage deglacial retreat of the southern Greenland Ice Sheet linked with Irminger Current warm water transport. *Paleoceanography*, *26*, doi:10.1029/2010PA002053

Korsgaard, N. J., Nuth, C., Khan, S. A., Kjeldsen, K. K., Anders, A., Schomacker, A., & Kurt, H. (2016). *Digital elevation model and orthophotographs of Greenland based on aerial photographs from 1978–1987* (G150 AERODEM) (NCEI Accession 0145405). Version 1.1. NOAA National Centers for Environmental Information. Dataset [19/09/2016].

Korsgaard, N. J., Nuth, C., Khan, S. A., Kjeldsen, K. K., Bjørk, A. A., Schomacker, A., & Kjær, K. H. (2016). Digital elevation model and orthophotographs of Greenland based on aerial photographs from 1978–1987. *Scientific Data*, *3*, 160032. doi:10.1038/sdata.2016.32

Lane, T. P., Roberts, D. H., Rea, B. R., Ó Cofaigh, C., & Vieli, A. (2015). Controls on bedrock bedform development beneath the Uummannaq Ice Stream onset zone, west Greenland. *Geomorphology*, *231*, 301–313. doi:10.1016/j.geomorph.2014.12.019

Larsen, N. K., Funder, S., Kjær, K. H., Kjeldsen, K. K., Knudsen, M. F., & Linge, H. (2014). Rapid early Holocene ice retreat in West Greenland. *Quaternary Science Reviews*, *92*, 310–323. doi:10.1016/j.quascirev.2013.05.027

Lea, J. M., Mair, D. W. F., Nick, F., Rea, B. R., van As, D., Morlighem, M., … Weidick, A. (2014). Fluctuations of a Greenlandic tidewater glacier driven by changes in atmospheric forcing: Observations and modelling of Kangiata Nunaata Sermia, 1859-present. *The Cryosphere*, *8*, 2021–2045. doi:10.5194/tc-8-2031-2014

Lea, J. M., Mair, D. W. F., Nick, F., Rea, B. R., Weidick, A., Kjær, K. H., … Schofield, J. E. (2014). Terminus-driven retreat of a major southwest Greenland tidewater glacier during the early 19th century: Insights from glacier reconstructions and numerical modelling. *Journal of Glaciology*, *60*(220), 333–344. doi:10.3189/2014JoG13J163

Lukas, S., & Bradwell, T. (2010). Reconstruction of a Lateglacial (Younger Dryas) mountain ice field in Sutherland, northwestern Scotland, and its palaeoclimatic implications. *Journal of Quaternary Science*, *25*, 567–580. doi:10.1002/jqs.1376

Motyka, R. J., Cassotto, R., Truffer, M., Kjeldsen, K. K., Van As, D., Korsgaard, N. J., … Rysgaard, S. (2017). Asynchronous behaviour of outlet glaciers feeding Godthåbsfjord (Nuup Kangerlua) and the triggering of Narsap Sermia's retreat in SW Greenland. *Journal of Glaciology*, *63*(238), 288–308. doi:10.1017/jog.2016.138

Murray, T., Scharrer, K., James, T. D., Dye, S. R., Hanna, E., Booth, A. D., … Huybrechts, P. (2010). Ocean regulation hypothesis for glacier dynamics in southeast Greenland and implications for ice sheet mass changes. *Journal of Geophysical Research*, *115*, F01005. doi:10.1029/2009JF001522

Nick, F. M., Vieli, A., Howat, I. M., & Joughin, I. (2009). Large-scale changes in Greenland outlet glacier dynamics triggered at the terminus. *Nature Geoscience*, *2*, 110–114. doi:10.1038/NGEO394

Nitsche, F. O., Larter, R. D., Gohl, K., Graham, A. G. C., & Khun, G. (2016). Bedrock channels in the Pine Island Bay, West Antarctica. In J. A. Dowdeswell, M. Canals, M. Jakobsson, B. J. Todd, E. K. Dowdeswell, & K. A. Hogan (Eds.), *Atlas of submarine glacial landforms: Modern, quaternary and ancient* (Vol. 46, pp. 217–218). London, Memoirs: Geological Society. doi:10.1144/M46.1

Paine, D. P., & Kiser, J. D. (2012). *Aerial photography and image interpretation* (3rd ed.). Hoboken, NJ: John Wiley & Sons. ISBN: 978-0-470-87938-2.

Pearce, D. (2014). *Reconstruction of Younger Dryas glaciation in the Tweedsmuir Hills, Southern Uplands, Scotland: Style, dynamics and palaeo-climatic implications* (Unpublished PhD thesis). University of Worcester.

Pearce, D., Rea, B. R., Bradwell, T., & McDougall, D. (2014). Glacial geomorphology of the Tweedsmuir Hills, Central Southern Uplands, Scotland. *Journal of Maps*, *10*(3), 457–465. doi:10.1080/17445647.2014.886492

Smith, M. J., & Wise, S. M. (2007). Problems of bias in mapping linear landforms from satellite imagery. *International Journal of Applied Earth Observation and Geoinformation*, *9*, 65–78. doi:10.1016/j.jag.2006.07.002

Spagnolo, M. J., Clark, C. D., Ely, J. C., Stokes, C. R., Anderson, J. B., Andreassen, K., … King, E. C. (2014). Size, shape and spatial arrangement of mega-scale glacial lineations from a large and diverse dataset. *Earth Surface Processes and Landforms*, *39*(11), 1432–1448. doi:10.1002/esp.3532

Taurisano, A., Billionøggild, C. E., & Karlsen, H. G. (2004). A century of climate variability and climate gradients from coast to ice sheet in west Greenland. *Geografiska Annaler: Series A, Physical Geography*, *86*(2), 217–224.

Taurisano, A., Bøggild, C. E., Schjøth, F., & Jepsen, H. (2003). Elevation change on the Greenland ice sheet at Qamanarssup Sermia, West Greenland. *Polar Geography*, *27*(1), 59–68. doi:10.1080/789610222

Tedstone, A. J., Nienow, P. W., Gourmelen, N., Dehecq, A., Goldberg, D., & Hanna, E. (2015). Decadal slowdown of a land-terminating sector of the Greenland Ice Sheet despite warming. *Nature*, *526*, 692–695. doi:10.1038/nature15722

Van As, D., Andersen, M. L., Petersen, D., Fettweis, X., Van Angelen, J. H., Lenaerts, J. T. M., … Steffen, K. (2014). Increasing meltwater discharge from the Nuuk region of the Greenland ice sheet and implications for mass balance (1960–2012). *Journal of Glaciology*, *60*(20), 314–322. doi:10.3189/2014JoG13J065

Van den Broeke, M., Bamber, J., Ettema, J., Rigot, E., Schrama, E., van de Berg, W. J., … Wouters, B. (2009). Partitioning recent Greenland mass loss. *Science*, *326*, 984–986. doi:10.1126/science.1178176

Vieli, A., & Nick, F. N. (2011). Understanding and modelling rapid dynamic changes of tidewater outlet glaciers: Issues and implications. *Surveys in Geophysics*, *32*(4), 437–458. doi:10.1007/s10712-011-9132-4

Weidick, A. (1959). Glacial variations in West Greenland in historical time Part I: South West Greenland. *Bulletin of the Greenland Geological Survey*, *18*, 196 Copenhagen University.

Weidick, A. (1963). Glacial variations in west Greenland in postglacial time. *International Association of Scientific Hydrology. Bulletin*, *8*(1), 75–82. doi:10.1080/02626666309493299

Weidick, A., Bennike, O., Citterio, M., & Nørgaard-Pedersen, N. (2012). *Neoglacial and historical glacier changes around Kangersuneq fjord in southern West Greenland*. Copenhagen: Geological Survey of Denmark and Greenland(ISBN: 978-87-7871-347-6). ISBN: 8778713471, 9788778713476.

Weidick, A., & Citterio, M. (2011). The ice-dammed lake Isvand (West Greenland) has lost its water. *Journal of Glaciology*, *57*(201), 186–188. doi:10.3189/002214311795306600

Woodroffe, S. A., Long, A. J., Lecavalier, B. S., Milne, G. A., & Bryant, C. L. (2014). Using relative sea-level data to constrain the deglacial and Holocene history of southern Greenland. *Quaternary Science Reviews*, *92*, 345–356.

Young, N. E., Briner, J. P., Hood, D. H., Finkel, R. C., Corbett, L. B., & Bierman, P. R. (2013). Age of the Fjord Stade moraines in the Disko Bugt region, western Greenland, and the 9.3 and 8.2 ka cooling events. *Quaternary Science Reviews*, *60*, 76–90. doi:10.1016/j.quascirev.212.09.028